J Mater Sci (2010) 45:5040–5044
DOI 10.1007/s10853-010-4455-y

ICAM 2009

Atomic packing and phase separation in Al-rare earth metallic glasses

Jerzy Antonowicz

Received: 30 November 2009 / Accepted: 29 March 2010 / Published online: 13 April 2010
© Springer Science+Business Media, LLC 2010

Abstract In this study, we discuss the origins of decomposition of the glassy phase in Al-rare earth melt-spun amorphous alloys. The small angle X-ray scattering results indicate that the amorphous phase undergoes phase separation by spinodal mechanism prior to devitrification. We recall a concept of Hume-Rothery of liquid immiscibility in binary liquid systems with strongly negative enthalpy of mixing. It is suggested that the experimental results may be explained by existence of an inflection in the Gibbs free energy curve of the amorphous phase due to effect of varying atomic packing efficiency with composition.

Introduction

Aluminium-rich binary Al–RE alloys [1] (RE=rare earth) are marginal glass formers with critical cooling rate for amorphization of order of 10^5 K/s typically achieved using melt spinning technique. Glass formation range (GFR) in this group of alloys is limited to a narrow composition range located at about 10 at.% of RE [2]. Al–RE metallic glasses are hypereutectic compositions with eutectic point located around 2–5 at.% of RE. During annealing, Al–RE metallic glasses crystallize in two or more stages during which fcc-Al and Al–RE intermetallic compounds precipitate from the amorphous matrix [3, 4]. For alloy compositions located in the Al-rich segment of the GFR, the first crystallization stage corresponds to primary transformation of fcc-Al phase. The resulting microstructure consists of ultra hight density ($\sim 10^{23}$ m^{-3}) of nanocrystalline grains with average size of around 10 nm embedded in the residual amorphous matrix [5]. Our recent studies of nanocrystallization in Al–RE metallic glasses [6–9] suggest that nanometer-scale amorphous phase separation prior to nucleation of crystalline fcc-Al is responsible for high nucleation frequency and limited growth of the nuclei. However, judging from the equilibrium phase diagram of Al–RE systems occurrence of phase separation seems rather unlikely.

In this work, we propose a mechanism, which may underlay phase separation in binary Al–RE metallic glasses. We recall a concept of Hume-Rothery [10] of liquid immiscibility in binary liquid systems with strongly negative enthalpy of mixing. According to this approach, a narrow miscibility gap may open near the composition corresponding to maximal atomic packing efficiency due to rapid dip in the Gibbs free energy curve (G-curve).

Experimental

Ingots of alloys considered in this study (nominal compositions $Al_{90}Y_{10}$, $Al_{92}Sm_8$, $Al_{91}Gd_9$, $Al_{91}Tb_9$, $Al_{90}Dy_{10}$) were prepared from pure elements using an arc-melting furnace. Samples in form of ribbons were produced in a melt-spinning device operating at wheel speed of 33 m/s in argon atmosphere. The ribbons were about 25-μm thick and about 2-mm wide. The small/wide angle X-ray scattering (SAXS/WAXS) measurements were performed at ID02 beamline of the European Synchrotron Radiation Facility (ESRF). Extended X-ray absorption fine structure (EXAFS) experiments were carried out at A1 station of HASYLAB facility. The technical details of SAXS/WAXS and EXAFS experiments and data processing were described in details elsewhere [7, 11, 12].

J. Antonowicz (✉)
Faculty of Physics, Warsaw University of Technology,
Koszykowa 75, 00-662 Warsaw, Poland
e-mail: antonowi@if.pw.edu.pl

SAXS/WAXS results

Both SAXS and WAXS signals originate from excess electron density and the difference between the two techniques is the range of the reciprocal space probed. The main advantage of the simultaneous SAXS and WAXS signals acquisition is a possibility of clear distinction between the crystallization process and compositional fluctuations on a nanometer scale in the amorphous phase. The presence of crystalline phases in the scattering volume is manifested by appearance of Bragg peaks on the "halo" diffraction pattern of the amorphous phase. On the other hand, the increase of the SAXS intensity is an evidence of compositional fluctuations in the sample. If no traces of crystallinity are present in WAXS while an intensity increase in SAXS is observed, one can conclude that the compositional inhomogeneities have amorphous character. In these kind of considerations, a value of minimal detectable crystalline volume fraction is a key parameter. In case of the experimental setup used for our measurements, the crystallinity detection threshold was as low as 0.05% volume fraction [8, 13].

Figure 1 presents the evolution of SAXS spectra during initial 32 min of annealing of amorphous $Al_{91}Gd_9$ alloy. The inset shows simultaneously taken WAXS spectra. A considerable increase of the SAXS intensity can be observed while WAXS spectra stay unchanged and exhibit a "halo" pattern with no traces of Bragg peaks. Judging from the q-position ($q = 4\pi\sin\theta/\lambda$ where λ is the incident beam wavelength and θ is half of the scattering angle) of the SAXS maximum, the characteristic wavelength of compositional fluctuations is about 10 nm. During further annealing, the Bragg peaks of fcc-Al nanocrystalline phase appear in the WAXS region, while SAXS maximum continues to grow and shift towards low q values [6, 7]. The above result is a clear evidence of presence of amorphous phase fluctuations appearing prior to nucleation of crystalline phases. Careful analysis of the experimental data shows that SAXS spectra evolution in early stages of transformation is in good agreement with Cahn's theory of spinodal decomposition [14], while the late stages follow so called "dynamical scaling" [15] behavior being a fingerprint of phase separation occurring by spinodal mechanism [16, 17].

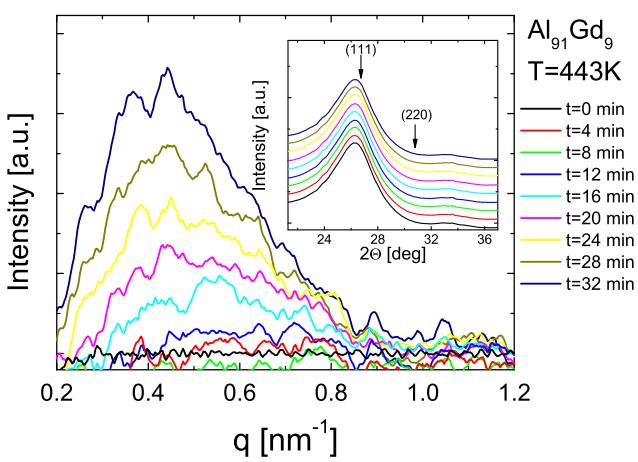

Fig. 1 Evolution of SAXS signal during initial 32 min of isothermal annealing (T=443K) of $Al_{91}Gd_9$ amorphous alloy. The *inset* shows simultaneously taken WAXS spectra giving evidence of completely amorphous character of the sample. Positions of (111) and (220) Bragg peaks belonging to the primary fcc-Al phase are indicated (For color version of this figure, the reader is referred to the online version of this article)

The result for $Al_{91}Gd_9$ alloy is representative also for other Al–RE alloys discussed in present study. A detailed discussion of SAXS/WAXS experimental data for both early and late stages of transformation as well as discussion of possible origins of observed SAXS results may be found in our previous works [6–9].

Structural features of Al–RE metallic glasses

Recently proposed structural models of metallic glasses [18, 19] are based on dense packing of solute-centered clusters. In case of binary Al-rich Al–RE amorphous alloys, the basic structural units of the glassy structure are RE centered clusters consisting of central RE atom surrounded closely by Al atoms [20]. The number of Al atoms in the first coordination shell of RE results from topological considerations of maximal allowed number of nearest neighbors for given R_{RE} to R_{Al} radii ratio. Values of R_{RE}/R_{Al} for different RE elements together with maximal topologically allowed coordination N_{max} (rounded down to integer) are listed in Table 1. The maximal solute coordination for all RE is equal to 17. The actual value of the RE coordination can be evaluated from EXAFS analysis [12, 21] of the amorphous alloys. The data obtained during EXAFS experiments N_{EXAFS} (Table 1) vary between systems, however, are close to the theoretical value of 17. As no EXAFS data are available for Al–Y alloy the N_{EXAFS} of

Table 1 Structural data and characteristic compositions for investigated Al-RE systems

Element	R_{RE}/R_{Al}	N_{max}	N_{EXAFS}	C_{DP}	$C_{\lambda=0.1}$	C this work
Y	1.259	17	14.1 ± 1.5	0.12 ± 0.01	0.10	0.10
Sm	1.259	17	14.8 ± 1.4	0.11 ± 0.01	0.10	0.08
Gd	1.234	17	18.0 ± 1.2	0.08 ± 0.01	0.11	0.09
Tb	1.231	17	15.8 ± 1.0	0.10 ± 0.01	0.11	0.09
Dy	1.238	17	18.5 ± 1.0	0.08 ± 0.01	0.11	0.10

The value of N_{EXAFS} for Al-Y alloy was taken from ref. [22]

yttrium was taken from anomalous X-ray scattering study of Matsubara et al. [22].

According to dense cluster packing approach, the medium range order in metallic glasses is realized by interconnection of clusters. Clusters share 12 of their outer solvent atoms to form an efficiently packed cluster structure involving fcc or hcp close packing [23] or icosahedral [19] symmetry. Assuming that the average cluster coordination is 12, one can calculate the solvent to solute atomic ratio S ($S = N/(1 + (12/N))$, where N is the solute coordination number). Solute concentration corresponding to the densely packed cluster structure $C_{DP} = 1/(S + 1)$ may be considered as the most stable configuration of the liquid and consequently glassy phase. Values of C_{DP} calculated for different Al–RE alloys from experimental N_{EXAFS} are given in Table 1. The minimum solute concentration C_{min} required for glass formation can be evaluated using topological instability model of Waseda and Egami [24]. According to this model, the solute concentration required to destabilize the solid phase and thus allowing amorphization is achieved when $\lambda = C|(R_{RE}/R_{Al})^3 - 1| \approx 0.1$, where λ is a topological instability parameter. Recently a quantitative criterion based on topological instability parameter was proposed for crystallization behavior of Al-based metallic glasses [25]. It was found that alloys with $\lambda < 0.1$ undergo primary nanocrystallization during annealing treatment while those with $\lambda > 0.1$ show eutectic crystallization into fcc-Al and intermetallic phases. The values of RE concentration corresponding to $\lambda = 0.1$ $C_{\lambda=0.1}$ as well as concentrations for alloys considered in this work are given in Table 1. It is worth to note that compositions of all investigated systems correspond to values of $\lambda \leq 0.1$. The graphical presentation of glass formation ranges (taken from [1]) and characteristic compositions values for different Al–RE systems is demonstrated in Fig. 2.

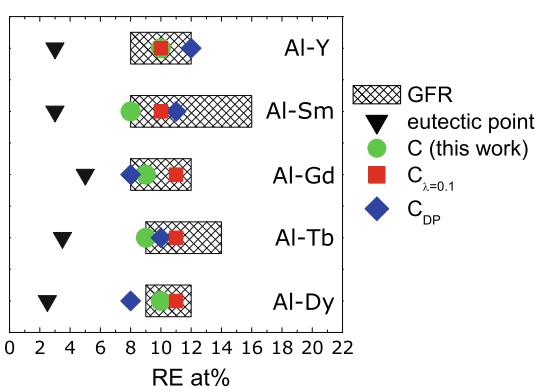

Fig. 2 Graphical presentation of glass formation ranges and characteristic compositions in Al–RE alloys. C—solute concentration for alloys considered in this work for which amorphous phase separation was observed, C_{DP}—solute concentration corresponding to the densely packed cluster structure, $C_{\lambda=0.1}$—solute concentration corresponding to $\lambda = 0.1$

As pointed out by Yavari [26], the dense cluster packing model of metallic glasses may be successful in predicting the distribution of eutectic points in binary phase diagrams (so called "Stockdale/Hume-Rothery puzzle") [10, 27]. As metallic glasses are usually formed near eutectic point, the composition of dense packing C_{DP} should coincide with the most favorable composition for glass formation. This concept was recently verified quantitatively by Shi et al. [28] by using the idealized atomic packing model for metallic glasses to predict the most stable metallic glasses and establish the correlation with eutectic points. Good statistical correlation between the predicted favorable compositions for metallic glass formation and eutectic points was found in case of symmetric eutectics. In case of asymmetric eutectics, the predicted compositions are off-eutectic. Authors of [28] argue that the actual glass formation range in case of asymmetric eutectics is located at compositions where the two T_0 lines cross the glass transition line. Al–RE metallic glasses are hypereutectic compositions and thus the optimal composition for glass formation corresponding to maximal packing efficiency is located at RE-rich side of equilibrium eutectic point.

Effect of atomic packing on thermodynamics of Al–RE amorphous alloys

The experimentally confirmed correlation between the dense packing of liquid and location of eutectics may be explained considering the effect of atomic packing density on shape of the liquid free energy curve. As suggested first by Hume-Rothery and Anderson [10], in a region of composition favorable for development of short- and medium-range order involving fivefold symmetry [29], the G-curve dips and thus more common tangents may be drawn, which makes occurrence of eutectic more likely. On the other hand, a rapid dip in the G-curve may result in inflection located on one or on both sides of C_{DP}. This effect is indeed observed in case of various binary systems with highly negative enthalpy of mixing and exhibiting a tendency towards ordering for specific composition. The examples of such systems are chalcogenides like Tl–Ta or Ag–Se having equilibrium miscibility gap or silica–alkai metal oxides like SiO_2–K_2O or SiO_2–NaO [30] having a metastable miscibility gap.

We suggest that mechanism similar to that described above may act in case of Al–RE amorphous alloys. The optimal composition for glass formation is located around 10 at.% of RE and similar solute concentration is obtained from purely geometrical considerations. The eutectics at Al-rich side of the phase diagram of Al–RE systems are

highly asymmetrical with the slope of liquidus on the side of intermetallic compound being much steeper than that on the side of fcc-Al phase. Thus, it may be expected that T_0 lines cross T_g line on the RE rich side of equilibrium eutectic point. The actual shape of the G-curve of the supercooled liquid/amorphous phase is not accessible for experimental reasons; however, one may expect that the G-curve would dip low for compositions of dense packing and thus favorable for glass formation. Following the idea of Hume-Rothery, it is reasonable to assume that the local lowering of free energy may contribute to inflection of the curve and thus to occurrence of a miscibility gap. The schematic presentation of a hypothetical form of the G-curve and the corresponding miscibility gap is shown in Fig. 3. In the model proposed here, the development of short-range order for compositions close to C_{DP} leads to lowering of the free energy and results in formation of a dip in the G-curve and a miscibility gap (A, B binodal points). For compositions close to C_{DP}, formation of amorphous phase is observed during rapid quenching of liquid. Between the binodal curves, a narrow spinodal region exists (C, D spinodal points). For an alloy with composition falling inside the spinodal region (NC—nanocrystal formation range), only sluggish kinetics prevents the systems from decomposition. If the atomic mobility is high enough, the alloy being in thermodynamically unstable state would undergo fine scale decomposition into two amorphous phases having solute concentrations A and B resulting from the common tangent construction. Al-rich phase (A) falls out of the GFR and undergoes crystallization, while RE-rich one (B) acts as the residual amorphous matrix. The above approach may shed light on the thermodynamic background of the λ criterion for crystallization behavior of Al-based glasses. At the same time, it can justify the appearance of fcc-Al as a primary product of devitrification given the thermodynamic calculations of driving force for crystallization indicate that the intermetallic should precipitate from the glassy phase on annealing [31].

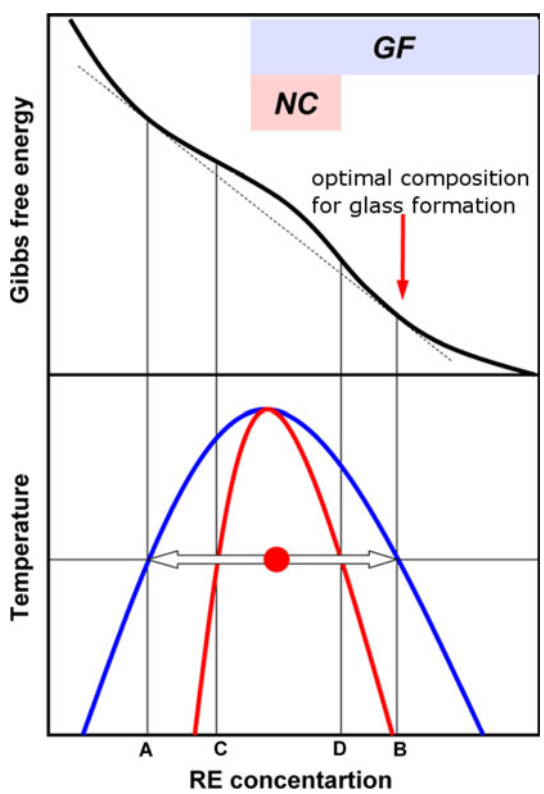

Fig. 3 Schematic presentation of a hypothetical form of the free energy curve and a metastable miscibility gap in Al–RE amorphous alloys. A and B define binodal points, compositions between C and D belong to a spinodal region. GFR—glass formation range, NC—nanocrystal formation range. For glass compositions falling into NC range spinodal decomposition and consequent nanocrystallization is observed on annealing

Summary

Recent findings suggest a correlation between the short-range order and thermodynamics of binary glass forming metallic systems. In this work, a mechanism relating the atomic packing to the shape of the Gibbs free energy curve is proposed to explain the experimental results indicating phase separation prior to crystallization of Al–RE amorphous alloys. It is proposed that lowering of free energy for compositions corresponding to dense atomic packing and thus favoring glass formation results in a dip producing an inflection in a G-curve. The inflection contributes to a narrow miscibility gap on the Al-rich side of the GFR. Alloys with compositions falling into the spinodal region undergo fine scale decomposition into two amorphous phases. Decomposition of the amorphous phase results in formation of a nanocrystalline microstructure consisting of fcc-Al nanocrystals embedded in an amorphous matrix.

Acknowledgements Author would like to thank professor A.R. Yavari for many valuable discussions. Doctor P. Panine and doctor M. Sztucki of the European Synchrotron Radiation Facility are acknowledged for their professional assistance in SAXS/WAXS measurements and experimental data interpretation.

References

1. Inoue A (1998) Prog Mater Sci 43:365
2. Zhu A, Shiflet G, Miracle DB (2004) Scr Mater 50:987
3. Rizzi P, Baricco M, Battezzati L, Schumacher P, Greer AL (1995) Mater Sci Forum 195:111
4. Pękała K, Latuch J, Jaśkiewicz P, Nowiński L, Antonowicz J (2004) J Metastable Nanocryst Mater 20–2:494
5. Wilde G, Wu RI, Perepezko JH (2001) In: 22nd Risø international symposium on materials science: science of metastable and nanocrystalline alloys: structure, properties and modelling, p 429

6. Antonowicz J, Yavari AR, Botta WJ, Panine P (2006) Philos Mag A 86:4235
7. Antonowicz J (2007) J Alloys Compd 434–435:126
8. Antonowicz J, Jezierska E, Kędzierski M, Yavari AR, Greer AL, Panine P, Sztucki M (2008) Rev Adv Mater Sci 18:454
9. Antonowicz J, Kędzierski M, Jezierska E, Latuch J, Yavari AR, Greer AL, Panine P, Sztucki M (2009) J Alloys Compd 483:116
10. Hume-Rothery W, Anderson E (1960) Philos Mag 5:383
11. Boesecke P (2007) J Appl Crystallogr 40:s423
12. Bacewicz R, Antonowicz J (2006) Scr Mater 54:1187
13. Panine P, Urban V, Boesecke P, Narayanan T (2003) J Appl Cryst 36:991
14. Cahn JW (1961) Acta Metall 9:795
15. Furukawa H (1984) Physica A 123:497
16. Binder K, Fratzl P (2001) Phase transformations in materials. Wiley-VCH, Weinheim
17. Fratzl P (2003) J Appl Cryst 36:397
18. Miracle DB (2006) Acta Mater 54:4317
19. Sheng H, Luo W, Alamgir F, Bai J, Ma E (2006) Nature 439:419
20. Miracle DB, Senkov ON (2003) J Non-Cryst Solids 319:174
21. Zalewski W, Antonowicz J, Bacewicz R, Latuch J (2009) J Alloys Compd 468:40
22. Matsubara E, Waseda Y, Inoue A, Ohtera H, Masumoto T (1989) Z Natur 44:814
23. Miracle DB (2004) Nat Mater 3:697
24. Egami T, Waseda Y (1984) J Non-Cryst Solids 64:113
25. de Sa Lisboa RD, Bolfarini C, Botta WJ, Kiminami CS (2005) Appl Phys Lett 86:211904
26. Yavari AR (2005) Nat Mater 4:104
27. Stockdale D (1935) Proc R Soc Lond A Math Phys Sci 152:81
28. Shi LL, Xu J, Ma E (2008) Acta Mater 56:3613
29. Frank FC (1952) Proc R Soc Lond A 215:43
30. Pelton A, Wu P (1999) J Non-Cryst Solids 253:178
31. Baricco M, Gaertner F, Cacciamani G, Rizzi P, Battezzati L, Greer AL (1998) Mater Sci Forum 269–272:553